Deformation Behavior of Isotactic Polypropylene Spherulite during Hot Drawing Investigated by Simultaneous Microbeam SAXS-WAXS and POM Measurement

Yoshinobu Nozue,*,† Yuya Shinohara,‡ Yasuo Ogawa,‡ Takashi Sakurai,† Hideaki Hori,† Tatsuya Kasahara,† Noboru Yamaguchi,† Naoto Yagi,§ and Yoshiyuki Amemiya‡

Petrochemicals Research Laboratory, Sumitomo Chemical Co., Ltd., Kitasode, Chiba, Japan; Department of Frontier Sciences, The University of Tokyo, Kashiwa, Chiba, Japan; and Japan Synchrotron Radiation Research Institute, Mikazuki, Hyogo, Japan

Received August 20, 2006; Revised Manuscript Received December 30, 2006

ABSTRACT: The process of rearranging lamella crystal structures in isotactic polypropylene (iPP) and butene randomly copolymerized iPP (bPP) spherulites during hot drawing was investigated by in-situ microbeam small-angle X-ray scattering (SAXS)−wide-angle X-ray scattering (WAXS)−polarized optical microscopy (POM) simultaneous measurements. We subjected a fixed position in an upper quadrant of a spherulite, which is stretched in the horizontal direction, to microbeam X-ray irradiation, and observed local structural changes, such as those in ordered crystal size and orientation, and a lamella stacking structure. We successfully obtained the structural information on parent and daughter lamellae in various orientations. In iPP, the long period of perpendicular parent lamellae increased, and then the disordering of crystal packing structures along the *a*-axis started. When necking started, the long periods of parent and daughter lamellae drastically started to decrease with the alignment of the *c*-axis in the stretching direction. The ease of crystal fragmentation and *c*-axis alignment strongly depended on the type of lamella, indicating the order of stress concentration during drawing. In bPP, it was found that the alignments of all the lamellae occur almost simultaneously and that parent and daughter lamellae independently rotate until necking.

Introduction

In polymer industries, polymer processing is one of the most important sections of research and development. Polymers are typically processed to films, bottles, fibers, and foams, and the mechanisms of polymer deformation have been vigorously studied by many researchers.[1−23] In particular, in the case of semicrystalline polymer processing, the comprehensive understanding of crystallization, orientation, and deformation of crystals under a force field is essential to a material design, and its related complex problems have also stimulated the interest of many researchers in the academic field.[1−21] To understand processes, such as inflation, injection molding, and T-die processing, which start from a completely molten polymer, the concept of flow-induced crystallization from a melt is essential, and many studies about flow-induced crystallization related to shish-kebab structural formation have been reported.[1−6] On the other hand, in processes, such as hot drawing and blow molding, in which crystallized polymers are heated to 10−30 °C below the melting point, partially melted and uni- or biaxially drawn, the concept of crystalline orientation rearrangement is very important. At a static field, semicrystalline polymers generally form hierarchical structures, such as a lamella stacking structure, a fibril structure (as a lamella bundle), and a spherulite. However, after hot drawing, polymers are highly fragmented and the *c*-axis is oriented in the stretching direction.[7−21] The first significant proposal about a structural deformation mechanism during drawing was made by Peterlin.[7] Peterlin reported that broken small crystalline blocks, which are connected by noncrystalline tie molecules, are highly oriented along the stretching direction and form a microfibril structure. Subsequently, some authors reported that melting and recrystallization are included in a transition scheme from crystal lamellae to a microfibril structure and proposed the mechanism by lamella crystals are partially melted under a strong tension, which is followed by recrystallization which results in a fibril structure upon further drawing.[8−12] However, the detailed mechanism of rearrangement from a spherulite to a fibril structure has been a controversial topic until now.[7−15,18,19]

Isotactic polypropylene (iPP), which is the material investigated in this study, is one of the representative polymers processed by drawing in order to obtain a thin film, and its deformation behavior is widely investigated.[16−21] To understand the rearrangement pathway of isotactic polypropylene crystals from spherulites to fragmented aggregates, the in-situ and ex-situ studies of spherulite structural deformation and rearrangement during drawing have been performed by various experimental techniques, such as infrared spectroscopy,[17,19] small-angle X-ray scattering (SAXS),[21] wide-angle X-ray scattering (WAXS),[19,21] and atomic force microscopy (AFM) measurements.[16] However, these techniques are insufficient for obtaining the local structural information during the deformation of crystals. For example, by infrared spectroscopy measurement, the formation of a higher-ordered structure cannot be observed, though we can obtain the information on the crystalline and amorphous chain anisotropies. By AFM, the information on crystal packing and the order of crystal orientation with a statistical accuracy cannot be obtained, whereas a change in higher-ordered structure at a surface can be observed qualitatively. In addition, the deformation behavior of a bulk region cannot be observed.

A combined SAXS-WAXS measurement is one of the most powerful tools in that it gives us the hierarchical structural

* Corresponding author. E-mail: nozue@sc.sumitomo-chem.co.jp.
† Sumitomo Chemical Co., Ltd.
‡ The University of Tokyo.
§ Japan Synchrotron Radiation Research Institute.

10.1021/ma061924v CCC: $37.00
Published on Web 02/15/2007

Table 1. Characteristics of Polymer Samples

sample	M_w	M_w/M_n	T_m[a]	T_c	comonomer	T_c(iso)[b]	T_m(iso)[c]	[*mmmm*]
iPP	440 000	4.8	160	117.5	non	128	168	0.91
bPP	414 000	3.8	159	117.2	butene 3 mol %	132	168	

[a] T_m is the nominal melting point determined by cool/heat scanning of DSC at 5 °C/min. [b] T_c(iso) is the isothermal crystallization temperature of the samples. [c] T_m(iso) is the melting point of the samples isothermally crystallized at T_c(iso).

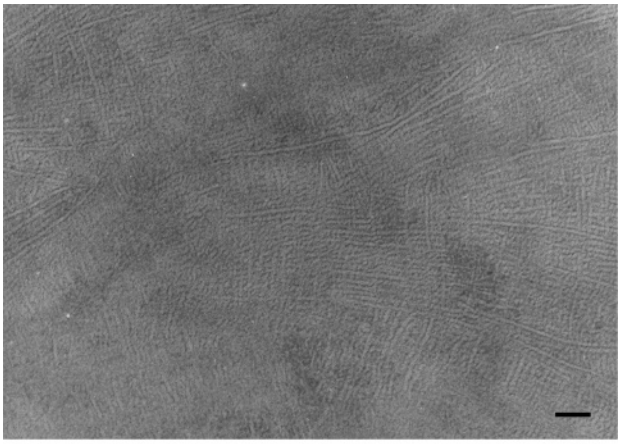

Figure 1. TEM images of isothermally crystallized samples after annealing at 155 °C (drawing temperature). In iPP (a), a uniformly distributed cross-hatched structure was observed. On the other hand, in bPP (b), the observed cross-hatched structure was highly disordered and nonuniformly distributed. Scale bars in the images are 1000 Å.

information on a wide scale, which ranges from the packing structure of crystals to lamella stacking, fibril structures. Furthermore, the use of a synchrotron radiation X-ray source enables us to perform a time-resolved measurement and to obtain a structural change on a millisecond time scale.[2,3,21,24−26] However, conventional X-ray beams have diameters of 0.1−2.0 mm in diameter, and the obtained structural information is spatially averaged, resulting in the insufficient information for constructing a local deformation model.

Recent third-generation synchrotron radiation sources aid in overcoming this problem by providing us with low-emittance X-rays. With this, we can obtain a microbeam of several microns diameter with a sufficiently low divergence and perform not only scanning[27−30] but also time-resolved microbeam SAXS-WAXS experiments.[31−34] In addition, two-dimensional X-ray detectors such as a CCD-based X-ray detector,[35,36] a flat-panel detector, and an imaging plate[37] enable us to perform a two-dimensional SAXS-WAXS simultaneous measurement.[38,39]

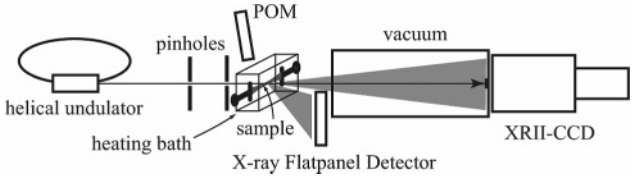

Figure 2. Experimental setup for in-situ microbeam SAXS-WAXS simultaneous measurement during hot drawing.

In this paper, to the extent of our knowledge, the first trial of in-situ microbeam SAXS-WAXS-polarized optical microscopy (POM) simultaneous measurement during the hot drawing of an isotactic polypropylene spherulite is reported. We have clearly observed the change in ordered crystal size and the rearrangement processes of four different types of lamella: parent lamellae with a parallel face (called "parallel parent lamellae") and a perpendicular face (called "perpendicular parent lamellae") with respect to the drawing direction, and their respective daughters. Furthermore, we have compared the deformation behavior of a large spherulite of isotactic polypropylene (iPP) with that of the isotactic polypropylene randomly copolymerized with a small amount of butene (bPP).

Experimental Methods

Materials. The iPP and bPP samples used in this study were obtained by polymerizing propene (and butene in the case of bPP) with a Ziegler−Natta catalyst. To obtain iPP and bPP with the same melt flow properties, the melt flow rates (MFRs) of iPP and bPP were adjusted by decomposition with peroxide. The characteristics of iPP and bPP are listed in Table 1. The molecular weight (M_w) and molecular weight distribution (M_w/M_n) were determined using a gel permeation chromatography apparatus (Millipore Waters 150-CV) at 145 °C. Three Shodex AT-806MS columns were used, and the solvent used was *o*-dichlorobenzene. The meso pentad ([*mmmm*]) of iPP was estimated by ^{13}C NMR (Bruker AVANCE-600) at a ^{13}C resonance frequency of 150 MHz at 135 °C. The *o*-dichlorobenzene solution with 10 wt % iPP was used for the ^{13}C NMR measurement. The analysis of meso pentad was performed by following the procedure described elsewhere.[40] The crystallization and melting temperatures (T_c and T_m) were determined by DSC (Seiko Instrument, EXSTAR6000). The iPP samples were first heated to 220 °C, held for 5 min, then cooled to 50 °C at a rate of 5 °C/min, and reheated to 180 °C at the same rate in a nitrogen atmosphere. In both crystallization and melting temperature determinations, the temperature at the peak position of the endothermic and exothermic heat flow chart during the cooling and the second heating were read out. The MFRs of the iPP and bPP samples at 230 °C were measured by the method specified in JIS K7210.

Sample Preparation for Drawing. The iPP and bPP samples were pressed at 230 °C for 5 min using a compact pressing machine and cooled to the temperature (T_c(iso)) shown in Table 1 and held at T_c(iso) for 10−12 h. Although it was not an isothermal crystallization in a strict sense, the induction periods of the iPP and bPP crystallizations at T_c(iso) were longer than the time when the temperature of the pressing machine reaches T_c(iso) (about 30 min), and an approximately isothermal crystallization was expected to proceed except for the central region of spherulites. The thickness of the obtained film was approximately 70−100 μm, and the diameters of isothermally crystallized spherulites were 200−300 μm. The melting temperatures of the isothermally crystallized iPP and bPP samples were measured by DSC with heating to 220 °C

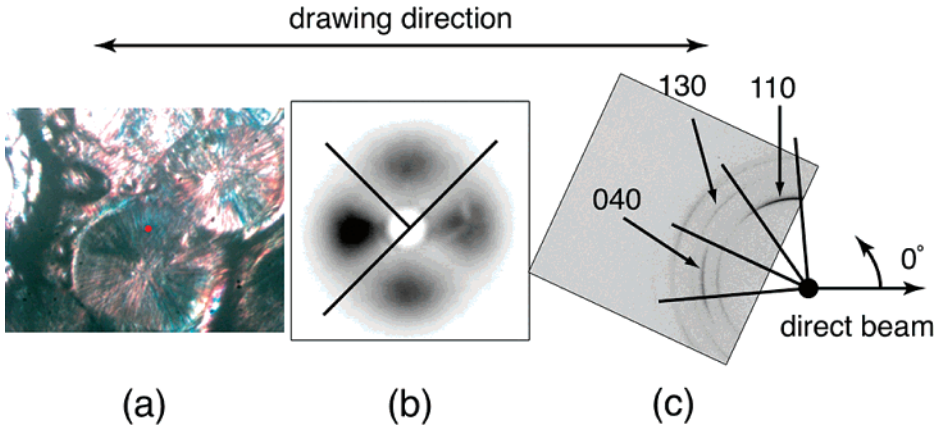

Figure 3. Typical data sets of POM (a), SAXS (b), and WAXS (c). In SAXS and WAXS, boundary solid lines for circular average analyses are shown. In the POM image, the position of the microbeam is shown by a red dot. The definition of azimuthal angle is shown in (c).

at a rate of 5 °C/min. To obtain a priori information on spherulite morphology, the TEM images of the iPP and bPP samples isothermally crystallized with annealing at 155 °C (drawing temperature) were obtained (Figure 1). In iPP, a clear cross-hatched structure was observed (Figure 1a). On the other hand, though the cross-hatched structure was also observed in bPP, the parent lamellae were more clearly observed than the daughter lamellae, and the cross-hatched structure was somewhat disordered and nonuniformly distributed (Figure 1b).

Before the drawing experiment, the crystallized film samples were cut into rectangles with a notch, and crossed tungsten wires with a diameter of 20 μm were attached to the samples by attaching adhesive tapes to the both edges of the long sides of the rectangles. The purpose of attaching the crossed tungsten wires was to determine the position of an X-ray microbeam before the drawing experiment. When the microbeam passed through a wire, a very strong streak pattern was observed. By determining the position at which the crossed streak pattern was observed, we obtained a rough estimate of the microbeam position. Once the rough estimate of the microbeam position was obtained under a microscope, it became easy to estimate accurately the microbeam position by irradiating the polymer samples with the X-ray microbeam without a 1/1000 absorber, which was inserted during the measurement, and by destroying the samples.

In-Situ Microbeam SAXS-WAXS-POM Simultaneous Measurement during Hot Drawing. The experiments were performed at BL40XU, SPring-8 (Hyogo, Japan). The experimental setup is schematically shown in Figure 2. The X-ray beam was quasi-monochromated ($\Delta E/E \sim 0.02$) using a helical undulator,[41] and a wavelength of 0.83 Å was used in this study. A microbeam was obtained by merely inserting a pinhole of 3 μm diameter at the 15 cm upstream of the sample position. Parasitic scattering was removed by the second pinhole of 50 μm diameter inserted just before the sample position. The beam size used in this study was about 4 μm × 4 μm in full width at half-maximum (fwhm), which was measured by scanning a Ta knife edge of 100 μm thickness. The position of the microbeam was observed by irradiating a linagraph paper.

The film sample was placed in a temperature-controlled uniaxial stretching machine. The drawing temperature was set at 155 °C in both iPP and bPP experiments. The sample was observed under an optical microscope, which was set without obstructing an X-ray path. The position at which the X-ray impinged, the elongation ratio and temperature of the sample were controlled outside the X-ray hutch. SAXS and WAXS images were simultaneously observed using a cooled CCD coupled with an X-ray image intensifier (XRII)[35] and an X-ray flat-panel imager (C9728DK, Hamamatsu Photonics Ltd., Japan), respectively. The sample-to-detector distances were about 2800 and 135 mm for SAXS and WAXS, respectively. The position of the X-ray beam was fixed in an upper region of a spherulite, when the spherulite was stretched in the horizontal direction. For data acquisition, the following procedure was repeated: (1) a sample was stretched while monitoring the POM image, (2) stretching was stopped, when any change was observed in the spherulite, (3) the sample position was adjusted so that a microbeam hits a fixed position in the spherulite, and (4) SAXS and WAXS images were simultaneously observed. The exposure time was 2 s for both SAXS and WAXS. The SAXS-WAXS measurement was performed within 20 s after stopping the stretching process. The stretching speed between chucks was 0.05 mm/s, and the initial distance between chucks was about 6 mm. However, in these experiments, drawing in a local region was observed and the rate of drawing speed in the local region of a spherulite was significantly different from the macroscopic drawing speed.

Analysis of SAXS Patterns. Figure 3b shows a raw SAXS pattern of PP, where a four-leaf clover pattern is observed. This pattern indicates that parent and daughter lamellae form a cross-hatched structure in an X-ray-irradiated region. The SAXS peaks observed in the vertical and horizontal directions originate from daughter and parent lamellae, respectively. To analyze the structural deformation of each lamella upon drawing, we divided the SAXS pattern into two parts as shown in the figure and circularly averaged the intensities of the two parts after Lorentzian correction. We fitted the obtained one-dimensional scattering profiles with Gaussian and then evaluated the long periods of lamellae and the fwhm of the profiles.

Analysis of WAXS Patterns. Figure 3c shows a typical raw WAXS pattern. As shown in this figure, only a partial pattern was obtained because the detector for WAXS was placed at an off-axis of the X-ray beam so as to record both SAXS and WAXS simultaneously. Four reflections, the 110 reflection of parent lamellae, 110 reflection of daughter lamellae, and the 040 and 130 reflections, were analyzed to investigate the structural change during drawing. Each reflection was azimuthally averaged after background subtraction and then fitted with Gaussian. The center position in the 2D WAXS pattern was determined so that the peak positions of the reflections along the radial direction should be consistent with each other. The azimuthal angle was defined as shown in the figure.

Relationship between Diffraction and Cross-Hatched Lamella Structure. To understand X-ray scattering patterns, we should consider both lamella and crystal axis orientations. In the case of iPP, it is well-known that the radial growth direction from the center of a spherulite is along the *a*-axis and that daughter lamellae grow by forming a *ca* lattice plane epitaxially on the well-matched *ac* lattice plane of parent lamellae[42,43] because the *a* and *c* lattice constants are very close to each other.[44] On the basis of this knowledge, we illustrate the relationship between parent and daughter lamellae in Figure 4. When we assign WAXS patterns to lamella structures in real space, we named the two representative lamellae of different orientations in Figure 4 parallel and perpendicular parent lamellae from the viewpoint of the stretching direction.

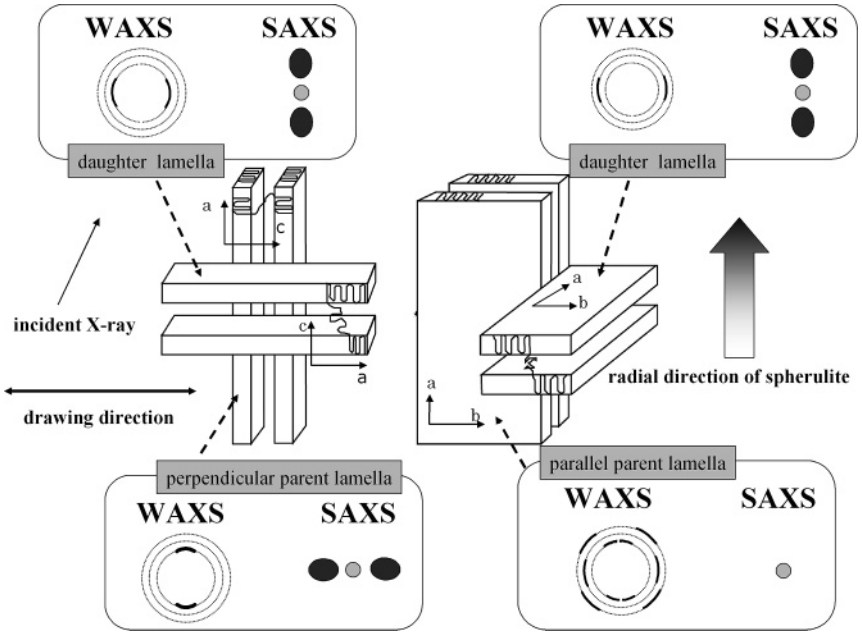

Figure 4. Illustrations of perpendicular and parallel parent lamellae and their daughter lamellae. The corresponding SAXS and WAXS are also shown.

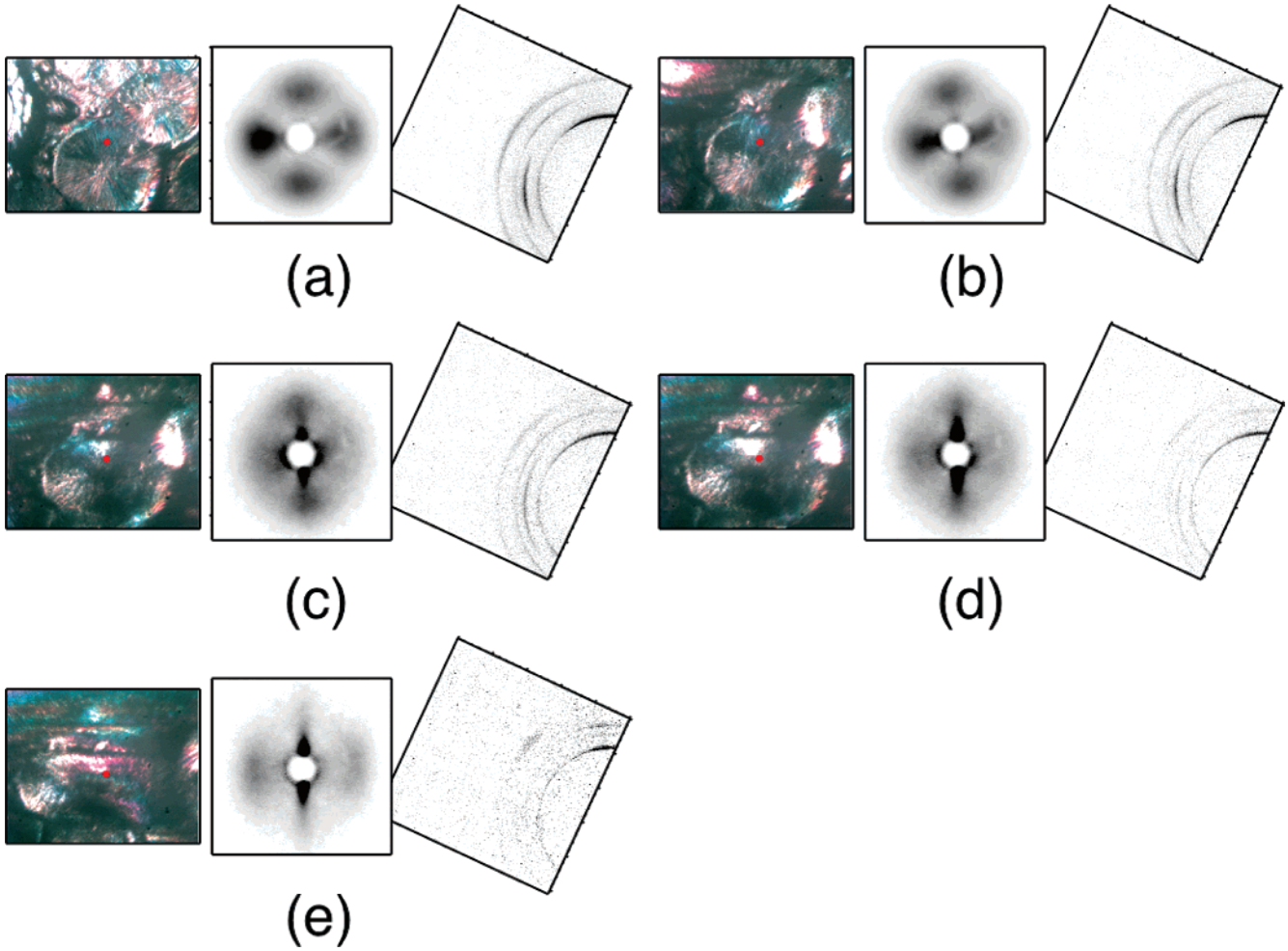

Figure 5. Representative POM-SAXS-WAXS data sets of iPP which were observed during hot drawing.

Results and Discussion

Microbeam SAXS-WAXS Pattern before Hot Drawing of iPP. The microbeam SAXS-WAXS patterns of iPP before hot drawing are shown in Figure 5a. In SAXS, a clear four-leaf clover pattern was observed, indicating that parent and daughter lamellae form a cross-hatched structure.[42,43] The SAXS intensities observed at 0° and 180° originate from parent lamellae, and those observed at about 90° and 270° originate from

daughter lamellae. Although the precise angle between a parent lamella and a daughter lamella should be 98°, the obtained scattering pattern is the superposition of 98° and 82°, resulting in the appearance of the scattering pattern at about 90°. In WAXS, the highly oriented 110, 040, and 130 reflections[30] due to the crystal orientation in the local region of the spherulite were observed. By referring to the illustration in Figure 4, the WAXS pattern in Figure 5a can be understood as follows: the 110 reflection of perpendicular parent lamellae appears as a two-spot pattern, namely, one spot at 90° and the other spot at 270°. Although the 110 reflection of parallel parent lamellae should appear as a four-spot pattern, two neighboring 110 reflections appear at 90° and 270° because the ratio of *a* to *b* is 3.15.[44] Therefore, the 110 reflection around 90° is the superposition from parent lamellae of various orientations including parallel and perpendicular parent lamellae. Accordingly, only one 110 reflection was observed at around 90° as the superposition of those of perpendicular and parallel parent lamellae in the partial WAXS image. On the other hand, the weak 110 reflection at around 180° originates only from the daughter lamellae grown from the perpendicular parent lamellae because the 110 reflection of the daughter lamellae grown from parallel parent lamellae does not satisfy the Bragg condition at all. Judged from the orientation of the *b*-axis in lamella planes described in Figure 4, the 040 reflection is the superposition of those of parallel parent lamellae and their daughter lamellae. The strong 130 reflection at 130° solely originates from parallel parent lamellae. The 130 reflection of parallel parent lamellae also appears as a four-spot orientation pattern, similar to the 110 reflection. However, perpendicular parent lamellae do not satisfy the Bragg condition for the 130 reflection. The weak 130 reflection observed at 180° is considered to originate from the daughter lamellae grown from parent lamellae which is aslant to the incident X-ray microbeam. With the above-mentioned consideration, we can obtain the valuable information on the rearrangement of respective lamella components by tracing the changes of the 110, 040, and 130 reflections in the azimuthal direction and their fwhm along the scattering angle.

In-Situ Microbeam SAXS-WAXS-POM Measurement during Hot Drawing of iPP. The changes observed in the SAXS-WAXS-POM image during the hot drawing of iPP are shown in Figure 5a−e. As shown in Figure 5, a fixed position of a spherulite was irradiated with a microbeam during hot drawing, and thus, the continuous structural changes in the fixed local region, the upper quadrant of the spherulite in this study, were traced.

First, we overview SAXS-WAXS-POM changes during hot drawing. In the initial stage shown in Figure 5b, the upper and lower parts of the spherulite were slightly deformed in the POM observation, as was reported previously for a polyethylene deformation at 100 °C.[45] Correspondingly, the SAXS characteristics of parent lamellae started to change before those of daughter lamellae did. The peak position of SAXS from perpendicular parent lamellae shifted to a smaller angle and its intensity decreased, whereas the peak position of SAXS from daughter lamellae remained the same though its intensity decreased. This indicates that the amorphous chains between perpendicular parent lamellae are elongated and that the long period of perpendicular parent lamellae increases, whereas that of daughter lamellae does not change. With respect to WAXS, the 110 reflection peak intensity at 180° decreased. This indicates that the disordering of daughter lamellae grown from perpendicular parent lamellae occurs at the beginning.

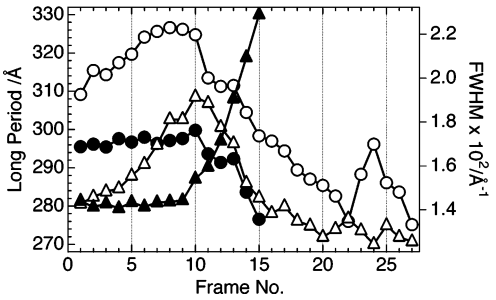

Figure 6. Changes in long period and fwhm in parent and daughter lamellae obtained from the circularly averaged SAXS profiles of iPP. Long periods of parent lamellae (open circles), long periods of daughter lamellae (filled circles), fwhms of parent lamellae (open triangles), and fwhms of daughter lamellae (filled triangles).

In the middle stage of deformation shown in Figure 5c,d, the POM image showed that the necking starts in the upper and lower quadrants of the spherulite. In this stage, the SAXS patterns showed that the scattering peak from the long period of lamellae along the stretching direction moves to a smaller angle (Figure 5c) and that it moves back to a wider angle afterward (Figure 5d), owing to the rearrangement of lamellae. The SAXS pattern from the stacking structure of daughter lamellae was also changed to a streaklike pattern. In the WAXS pattern in Figure 5c, all the reflections were highly broadened in the azimuthal direction, strongly indicating the disordering of crystalline orientation during deformation, and then the rearrangement of crystals in the *c*-axis orientation along the stretching direction started to develop in Figure 5d.

In the late stage of deformation shown in Figure 5e, the scattering intensity from the long period simply increased, indicating the progress of rearrangement. WAXS became more anisotropic, indicating that the rearrangement of crystals in the *c*-axis orientation along the stretching direction develops further.

Next, we evaluate the changes observed in SAXS-WAXS patterns during hot drawing in more detail. To quantitatively understand the changes in the long periods of parent and daughter lamellae, we show the changes in the long period and fwhm of SAXS peaks during hot drawing in Figure 6; the long period of parent lamellae initially increased, then temporarily remained at the maximum value, and finally markedly decreased when necking started. It is noted that a long period shorter than that before hot drawing was finally reconstituted. The fwhm of the SAXS profile from parent lamellae increased and showed a maximum value just when the marked decrease in long period started. This strongly indicates that the disordering of the long period of perpendicular parent lamellae continuously progresses until the initial stage of necking, followed by their ordering. On the other hand, the long period of the daughter lamellae did not change in the initial stage unlike that of perpendicular parent lamellae, and then it simply decreased and finally disappeared when necking started. Correspondingly, the fwhm of the SAXS peak from daughter lamellae did not change either in the initial stage and then simply increased until the SAXS peak disappeared.

To quantitatively understand the WAXS change during hot drawing, we first calculated the azimuthal intensity distribution profiles of the 110, 040, and 130 reflections and showed their changes as bird's-eye view (Figure 7). From Figure 7, the following phenomena can be observed: the 110 reflection observed at around 180° disappeared first, followed by the azimuthal distribution change of the 130 reflection, and finally by that of the 040 reflection. It should be noted that the 110 reflection at 90° remained with its width narrowed in the

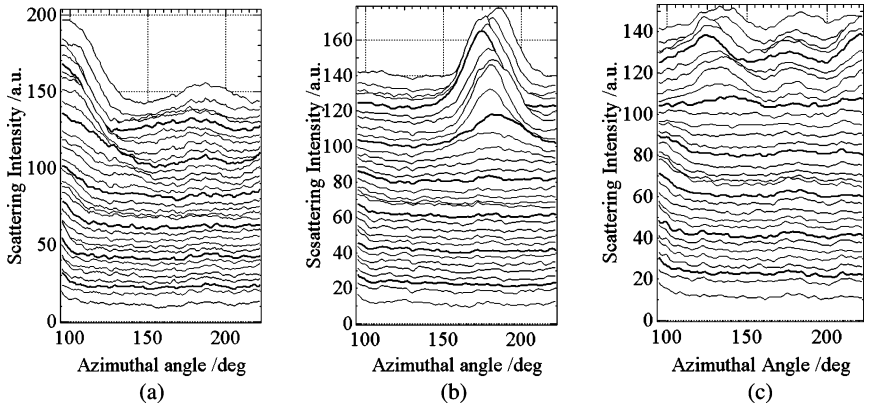

Figure 7. Bird's-eye views of changes in azimuthal distributions of (a) 110, (b) 040, and (c) 130 reflections of iPP. At every five frames, profiles are shown by a bold lines. Time advances from top to bottom.

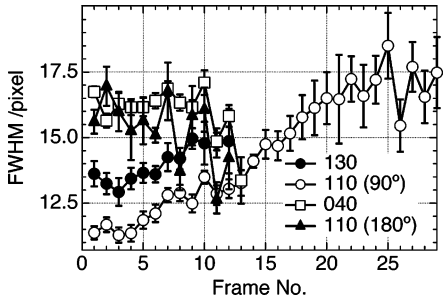

Figure 8. Changes in fwhms of 110, 040, and 130 reflections of iPP during hot drawing. With respect to the 110 reflection, both reflections at 90° (corresponding to perpendicular and parallel parent lamellae) and 180° (corresponding to daughter lamellae of parallel parent lamellae) were analyzed.

azimuthal direction during hot drawing. This indicates that the lamella plane rotates and is rearranged in the *c*-axis orientation along the stretching direction, sequentially depending on the type of lamella. Furthermore, we also analyzed the changes in the fwhms of the 110 reflections at around 90° and 180°, the 040 reflection at around 180°, and the 130 reflection at around 135° from circularly averaged one-dimensional profiles during hot drawing (Figure 8). It is well-known that the fwhm of the X-ray reflection from the crystal plane is inversely proportional to the number of periodic planes, which is approximated as the ordered crystal size in the direction normal to the corresponding plane, and thus, we can obtain the change in ordered crystal size during hot drawing. From Figure 8, it is clearly observed that the fwhm of the 110 reflection at 180° gradually decreases and that of the 110 reflection at 90° accordingly increases first (see frames 4−10). Also, the increase in the fwhm of the (130) plane of parallel lamellae occurs simultaneously. Interestingly, the ordered crystal sizes of the (040) planes of parallel parent lamellae and their daughter lamellae start to increase from frame 10. Furthermore, by comparing the fwhm of the long period of daughter lamella shown in Figure 6 with that of the 040 reflection in Figure 8, it is found that the decrease in the fwhm in the (040) plane starts simultaneously with the increase in the fwhm of the long period of daughter lamellae after the fragmentation of the (130) plane.

iPP Structure Deformation during Hot Drawing. On the basis of the experimental results shown above, we propose a structural deformation model of iPP during hot drawing, which is illustrated in Figures 9 and 10. In the first stage of hot drawing (frames 1−3 in Figures 6 and 8), the elongation of amorphous chains between perpendicular parent lamella crystals seems to occur (Figure 9b). This is evidenced by the increase in the long

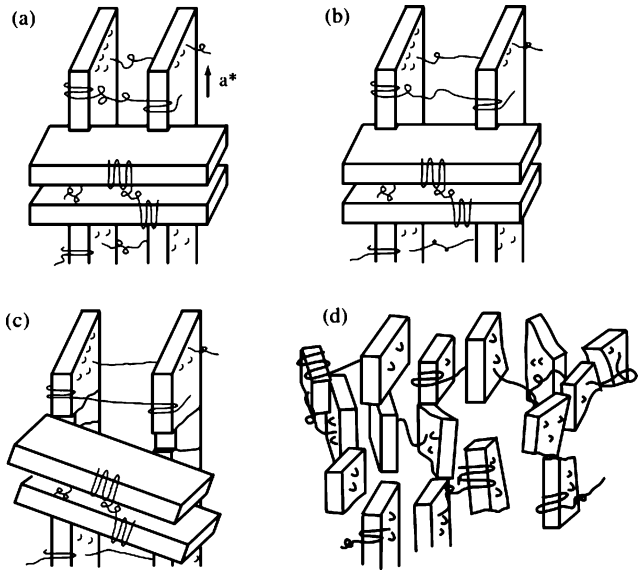

Figure 9. Deformation model of perpendicular lamellae in iPP: initial state (a), elongation of amorphous chain at first stage (b), disordering of parent lamella crystal along *a*-axis and rotation of daughter lamellae at second stage (c), and fragmentation at final stage (d).

period of perpendicular parent lamellae observed in SAXS without any other changes in SAXS and WAXS.

In the second stage of hot drawing (frames 4−9 in Figures 6 and 8), the following two phenomena seem to occur: (1) the gradual rotation of their daughter lamellae with small crystals (Figure 9c) and (2) the breaking of parallel parent lamellae, which makes the ordered crystal size along the *a*-axis become smaller (Figure 10b). Phenomenon (1) is evidenced by the disappearance of the 110 reflection at around 180°, resulting in the appearance of the broadening parts of the 110 reflection at around 90° in WAXS. It is also evidenced by the decrease in the fwhm of the 110 reflection around 180°. Phenomenon (2) is evidenced by the increase in the fwhm of the 130 reflection despite no change in the fwhm of the 040 reflection. This model in the first and second stages seems to be reasonable from the following viewpoints. Initially, the amorphous regions of perpendicular parent lamellae are expected to be strongly affected by the external force field, and the daughter lamellae connected to their parent lamellae are expected to be stressed in response to the increase in distance between perpendicular lamellae, being rotated into align the *c*-axis of the crystals parallel to the stretching direction. The daughter lamellae with small crystal are expected to be more easily rotated, and those with large crystals are expected to remain without rearrange-

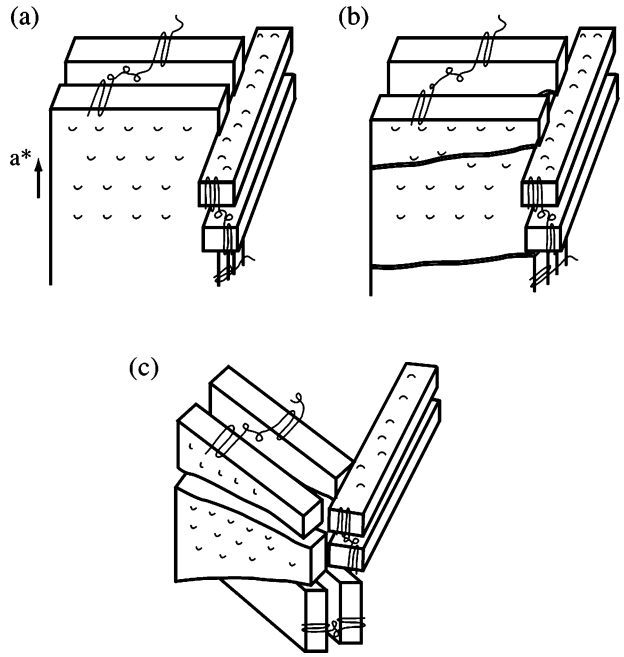

Figure 10. Deformation model of parallel lamellae in iPP: initial stage (a), disordering of crystal along *a*-axis (b), and rotation of parent lamellae followed by rotation of daughter lamellae (c).

ment. Together with the elongation of amorphous chains between perpendicular parent lamella crystals and the rotation of their daughter lamellae, parallel parent lamellae start to be stressed by the external force field. On the other hand, the daughter lamellae grown from parallel parent lamellae are expected not to be affected by the force field in the initial stage. Note that this is evidenced by the unchanged fwhm of the 040 reflection and the unchanged SAXS peak position from daughter lamellae until the second stage. The following would be a conceivable factor that may explain the reason why the ordered crystal size of parallel parent lamellae along the *a*-axis decreases. Generally, a large structure and a structure with a high aspect ratio are subject to shear stress, which is caused by a microscopically inhomogeneous force. Initially, the lamella plane size is much larger along the *a*-axis than along the *b*-axis, which is caused by the primary crystal growth along the *a*-axis (in the radial direction), that is, a high aspect ratio between the *a*- and *b*-axes. Furthermore, the region of the junction points of the cross-hatched structure would result in a much higher aspect ratio than the other region.

In the third stage of hot drawing (frames 10−15), parallel fragmented parent lamellae start to align the *c*-axis parallel to the stretching direction (Figure 10c), and then the rotation of the daughter lamellae grown from parallel parent lamellae starts to occur. This is evidenced by the changes in the azimuthal distributions of the 130 and 040 reflections. The former proceeds the latter by three frames. Simultaneously, the ordering of lamella stacking structures in oriented lamellae with the *c*-axis parallel to the stretching direction also starts.

In the fourth stage (frames 16−29), the structural change is simple, and the orientation order of fragmented lamella blocks increases (Figure 9d), which is evidenced by the increasing anisotropy of the SAXS-WAXS pattern.

From our experimental results, we cannot find the clear evidence of melting and recrystallization, and it is reasonable to consider that the rearrangement pathway of crystal blocks during hot drawing does not include melting and recrystallization as dominant mechanisms. Instead of melting and recrystallization, the fragmentation and rotation of lamellae in the spherulite in the second and third stages are the most essential processes for the iPP drawn under our experimental conditions (slow drawing). We can suppose that the drawing speed of our experiment is below the critical speed which induces melting and recrystallization that is an ultimate state of fragmentation, though we should investigate the effect of the stretching speed on the fragmentation of lamellae in the future. Also, we cannot exclude the possibility of melting and recrystallization in the very local region, which is proposed in the switchboard model,[11] because of our detection limit.

Microbeam SAXS-WAXS Pattern before Hot Drawing of bPP. As shown in Figure 11a, the SAXS-WAXS patterns of bPP before hot drawing are different from those of iPP. In SAXS, the relationship between parent and daughter lamellae is not orthogonal, whereas a complete four-leaf clover like pattern is observed in iPP. In WAXS, the relationships of the azimuthal intensity distributions among the 110, 040, and 130 reflections are different between iPP and bPP.

In-Situ Microbeam SAXS-WAXS-POM Measurement during Hot Drawing of bPP. The result obtained by the microbeam SAXS-WAXS-POM of bPP during hot drawing were analyzed in the same manner as that in the case of iPP. The SAXS-WAXS-POM images obtained during the hot drawing of bPP are shown in Figure 11a−g. The continuous structural changes in the fixed local region, the upper quadrant of a bPP spherulite, were traced with a microbeam.

First, we overview SAXS-WAXS-POM changes during hot drawing. In the initial stage, as shown in Figure 11b, the shape of the spherulite was slightly deformed in the POM observation. Interestingly, the relative azimuthal angle between SAXS peaks from parent and daughter lamellae was gradually changed (Figure 11a−c). Correspondingly, the relationship of the azimuthal intensity distribution among the 110, 040, and 130 reflections in the WAXS pattern was also changed. As is shown by SAXS in Figure 11c, further drawing induced the disordering of parent lamella stacking structures followed by that of daughter lamella stacking structures. The peak position of SAXS from perpendicular parent lamellae shifted to a smaller angle and its intensity decreased, whereas that of SAXS from daughter lamellae remained the same. With respect to WAXS in Figure 11c, all the reflections were broadened in the azimuthal direction. In the initial stage of necking corresponding to Figure 11d,e, the changes in the intensity and azimuthal position of SAXS were rather complicated. With respect to WAXS in Figure 11d,e, the broadening of the reflections in the azimuthal direction continued. In Figure 11f,g corresponding to the stage of further necking, the rearrangement of lamella structures in the *c*-axis orientation along the stretching direction proceeded in SAXS. However, in WAXS, the initial azimuthal intensity distribution partially remained, whereas the azimuthal intensity distribution corresponding to the *c*-axis orientation along the stretching direction increased.

Next, we evaluate the changes observed in SAXS-WAXS patterns during hot drawing in more detail. To quantitatively understand the changes in the long period of parent and daughter lamellae, we show the changes in the long period and fwhm of SAXS profiles during hot drawing in Figure 12. The changes in the long period and fwhm of parent and daughter lamellae in bPP are similar to those in iPP. That is, the disordering of the long period of perpendicular parent lamellae progressed in the initial stage of deformation, followed by their reordering. On the other hand, the long period of daughter lamellae, unlike that of their perpendicular parent lamellae, remained in the initial

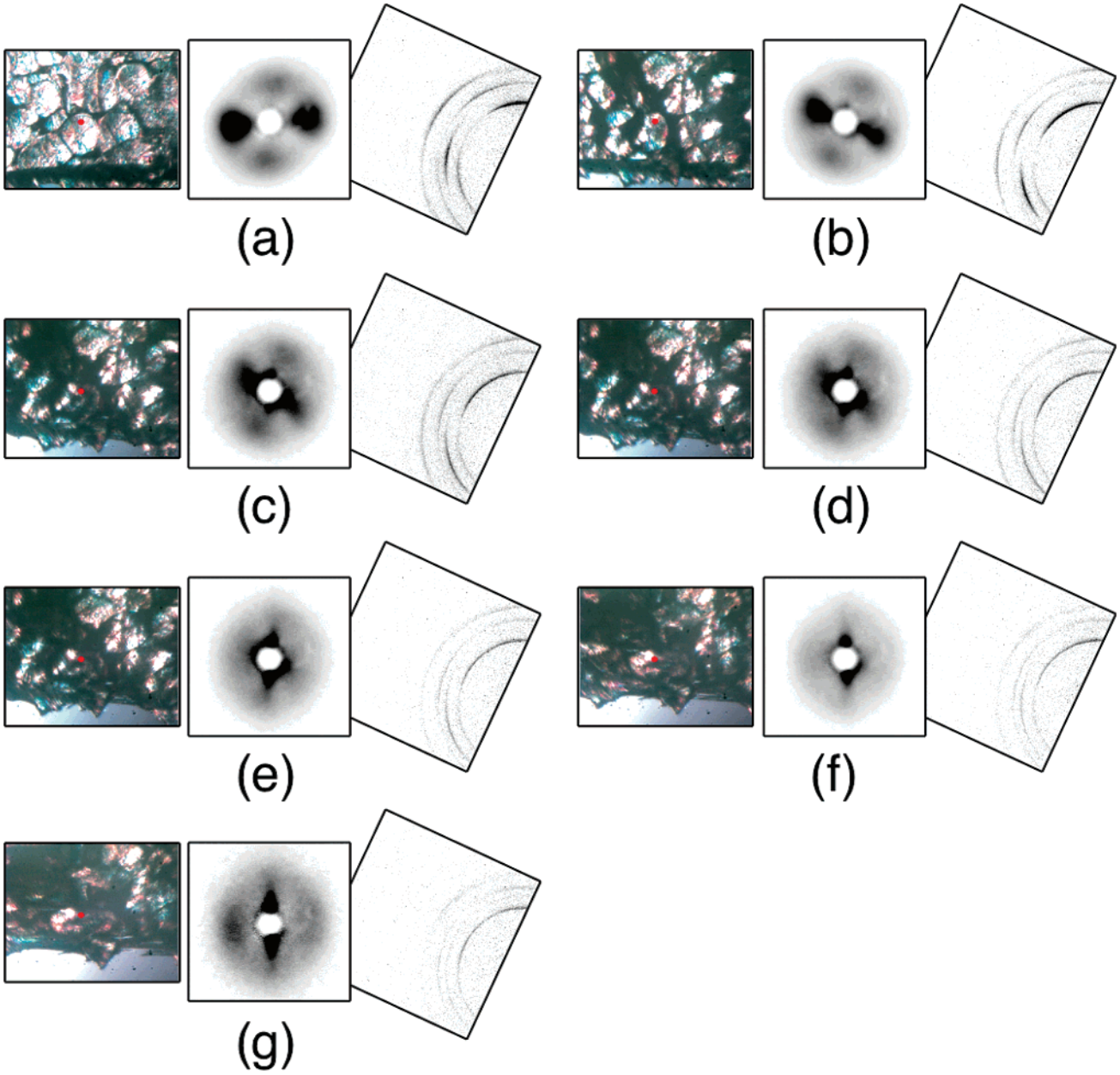

Figure 11. Representative POM-SAXS-WAXS data sets of bPP observed during hot drawing.

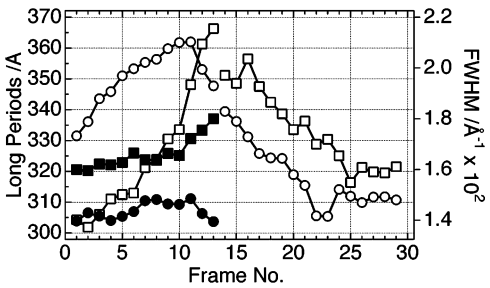

Figure 12. Changes in long periods and fwhms of parent and daughter lamellae obtained from circularly averaged SAXS profiles of bPP: long period of parent lamellae (open circles), long period of daughter lamellae (closed circles), fwhm of parent lamellae (open squares), and fwhm of daughter lamellae (closed squares). In the case of bPP, the region for analysis was determined frame by frame because each reflection largely moved in the azimuthal direction during drawing.

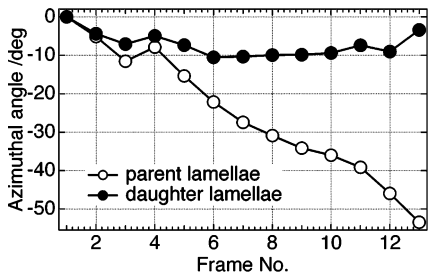

Figure 13. Rotations of SAXS peak positions of parent and daughter lamellae of bPP in azimuthal direction during hot drawing. This indicates that the parent and daughter lamellae independently move.

stage, then simply decreased, and finally disappeared when necking started. Correspondingly, the fwhm of the SAXS peak from daughter lamellae did not change in the initial stage and then simply increased until the SAXS peak disappeared. In the case of bPP, the change in the azimuthal position of SAXS from parent and daughter lamellae was analyzed in detail. In Figure 13, the relative changes in the azimuthal angles of the SAXS peak positions from parent and daughter lamellae during hot drawing are plotted. It is clearly observed that the azimuthal rotations of parent and daughter lamellae seem to be independent

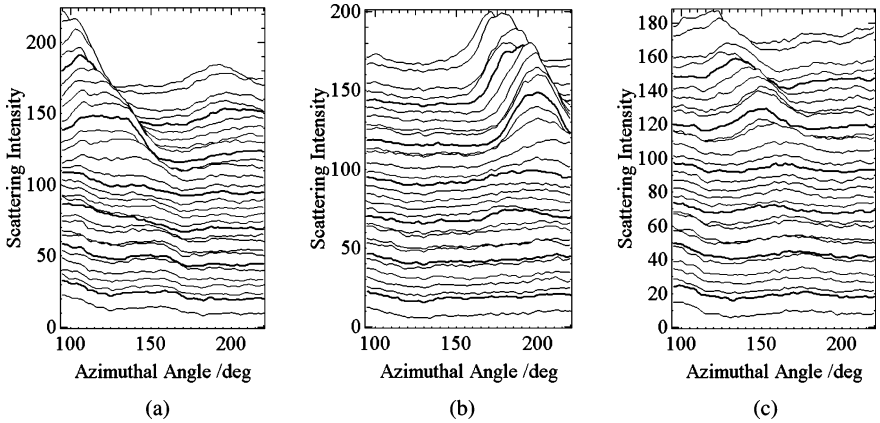

Figure 14. Bird's-eye view of changes in azimuthal distributions of (a) 110, (b) 040, and (c) 130 reflections of bPP. At every five frames, profiles are shown by bold lines.

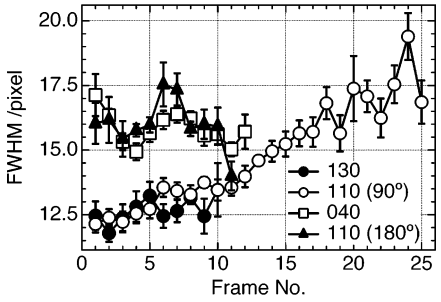

Figure 15. Changes in fwhms of 110, 040, and 130 reflections of bPP during hot drawing. With respect to the 110 reflection, both reflections corresponding to parent lamellae and daughter lamellae of parallel parent lamellae were analyzed. In the case of bPP, the region for analysis was determined frame by frame because each reflection largely moves in the azimuthal direction during drawing.

of each other from frame 5. The seemingly cooperative rotations in the first five frames are due to the rotation of the entire spherulite, which we observed by POM. This result indicates that the connection between parent and daughter lamellae is much weaker in bPP than in iPP.

We calculated the azimuthal intensity distribution profiles of the 110, 040, and 130 reflections and showed their changes as a bird's-eye view (Figure 14). From Figure 14, the following interesting characteristics of bPP, which is different from those of iPP, can be observed: (1) The azimuthal distributions of the 110, 040, and 130 reflections change almost simultaneously, indicating that the rearrangement of crystals in the *c*-axis orientation along the stretching direction occurs simultaneously in all the lamellar crystals. (2) Some crystals remained in the initial orientation even when necking started. Furthermore, we also analyzed the fwhms of the 110, 040, and 130 reflections along the scattering angle of circularly averaged one-dimensional profiles during hot drawing (Figure 15). Before hot drawing, the fwhm of daughter lamellae is much larger than that of parent lamellae, indicating that the ordered crystal size of daughter lamellae is much smaller than that of parent lamellae. In the initial stage (frames 1−5), the fwhms of the 130 and 110 reflections at 90° gradually increase. In the following stage (frames 6−10), the fwhms seem to be unchanged. Then, the fwhm of the 110 reflection at 180° markedly decreases at frame 11, whereas that of the 110 reflection at 90° gradually increases. By comparing the rotation of the long period in the azimuthal direction shown in Figure 13 with the fwhms of the 110, 040, and 130 reflections in Figure 15 in detail, it was found that the ordered crystal sizes along the ⟨040⟩ and ⟨110⟩ at 180° remain for a while (frames 5−9), in which the long periods of parent and daughter lamellae independently moved in the azimuthal direction.

bPP Structure Deformation during Hot Drawing. From the above experimental results, we discuss the structural deformation of bPP during hot drawing. In the case of the bPP spherulite, the correlation between parent and daughter lamellae, which forms the cross-hatched structure, is very weak, and parent and daughter lamellae independently respond to the external force. Such a response is evidenced by the independent azimuthal rotation of the SAXS peak position.

In the initial stage of hot drawing (frames 1−5 in Figures 12 and 15), the decrease in ordered crystal size along ⟨110⟩ and ⟨130⟩, which may be caused by the breaking of crystals, proceeded slowly and continuously together with the increase in distance between perpendicular parent lamella crystals. In the following stage until necking (frames 5−10), the ordered crystal size hardly changed, the distance between perpendicular parent lamella crystals continued to increase, and parent and daughter lamellae independently rotated.

In the middle stage (frames 11−16) corresponding to the start of necking, parent and daughter lamellae simultaneously rearranged in the *c*-axis (see Figure 14) along the stretching direction. In addition, the ordered crystal size of the daughter lamellae of perpendicular parent lamellae along the ⟨110⟩ increased during this process. Furthermore, some of the crystalline blocks remained in the original orientation and were not rearranged when necking started.

In the late stage of hot drawing (frames 16−29), although the rearrangement of crystal blocks in the *c*-axis orientation along the stretching direction further proceeded, the remaining crystal blocks in the middle stage still existed.

The above-mentioned deformation behavior is expected to be explained by the nonuniform cross-hatched structure observed by TEM and by the knowledge with respect to the crystal structure that a butene comonomer is incorporated into the crystal region, resulting in the expansion of the crystal packing structure.[46] It is supposed that the incorporation of the butene into the crystal region causes the structural instability of bPP crystals because the incorporated butene is expected to be a type of defect or a destabilizer of crystal packing. Many defects in bPP crystals are expected to induce the breaking of the crystals by the external force, and bPP lamella crystals are expected to be easily fragmented. The easy fragmentation and disordered and nonuniform cross-hatched structure of bPP lamella crystals may induce not only the independent movements of parent and daughter lamella blocks but also the simultaneous breaking and rearrangement of crystalline lamellae

oriented in various directions. Furthermore, the very weak connection between parent and daughter lamellae is also expected to allow some fragmented lamella blocks to remain in the original orientation.

Whereas the WAXS pattern shows a weakly anisotropic pattern, a highly anisotropic pattern is observed in SAXS. This indicates that the remaining crystals without alignment of the crystal *c*-axis parallel to the stretching direction have no stacking structure and are isolated.

Summary of Difference of Deformation between iPP and bPP. The structural deformation of iPP and bPP during hot drawing discussed above is summarized in this section.

The common features of iPP and bPP deformations during hot drawing are as follows: Until necking, the long period of perpendicular parent lamellae increases and reaches a constant value, while that of daughter lamellae does not change. When necking starts, the long periods of parent and daughter lamellae simultaneously start to decrease with the alignment of the *c*-axis in the stretching direction.

The characteristic features of iPP deformation during hot drawing are as follows: (1) The alignment of the *c*-axis in the stretching direction proceeds in a sequential order. First, the daughter lamellae grown from perpendicular parent lamellae, followed by parallel parent lamellae, and finally the daughter lamellae grown from parallel parent lamellae are rearranged. (2) The long period of daughter lamellae does not change while keeping the angle fixed between parent and daughter lamellae.

The characteristic features of bPP deformation during hot drawing are as follows: (1) Parent and daughter lamellae rotate independently during hot drawing until necking starts. (2) The rearrangements of all the parent and daughter lamella planes, which result in the *c*-axis orientation along the stretching direction, simultaneously occur when necking starts. Furthermore, some crystalline blocks remain in the original orientation even after necking starts.

Conclusion

We have performed in-situ microbeam SAXS-WAXS-POM simultaneous measurements during the hot drawing of iPP and bPP spherulites. We have successfully separated the structural information on parent and daughter lamellae in various orientations. In these experiments, we have obtained the detailed information on the subsequent disordering (fragmentation and rotation) processes of lamella stacking and crystal planes and the rearrangement process of disordered lamella blocks during necking. We have also learned the essential difference in deformation manner between iPP and bPP and discussed it on the basis of their crystal structures. This study has demonstrated that a microbeam SAXS-WAXS-POM simultaneous measurement is a unique and powerful tool for investigating a local structural change when an external force is applied to polymers.

Acknowledgment. The authors thank Dr. Katsuaki INOUE (JASRI) and Dr. Noboru OHTA (JASRI) for supporting us in setting up the microbeam experiment. This experiment was performed under the approval of the SPring-8 Program Advisory Committee (Proposal No.: 2005A0705, 2005B0155). Preliminary μ-beam SAXS/WAXS experiments were performed under the approval of the Photon Factory Program Advisory Committee (Proposal No. 2004G268).

References and Notes

(1) Seki, M.; Thurman, D. W.; Oberhauser, J. P.; Kornfield, J. A. *Macromolecules* **2002**, *35*, 2583.
(2) Somani, R. H.; Yang, L.; Hsiao, B. S.; Agarwal, P. K.; Fruitwala, H. A.; Tsou, A. H. *Macromolecules* **2002**, *35*, 9096.
(3) Yang, L.; Somani, R. H.; Sics, I.; Hsiao, B. S.; Kolb, R.; Fruitwala, H.; Ong, C. *Macromolecules* **2004**, *37*, 4845.
(4) Azzurri, F.; Alfonso, G. C. *Macromolecules* **2005**, *38*, 1723.
(5) Zhang, X. M.; Elkoun, S.; Ajji, A.; Huneault, M. A. *Polymer* **2004**, *45*, 217.
(6) Nogales, A.; Hsiao, B. S.; Somani, R. H.; Srinivas, S.; Tsou, A. H.; Balta-Calleja, F. J.; Ezquerra, T. A. *Polymer* **2001**, *42*, 5247.
(7) Peterlin, A. J. *J. Mater. Sci.* **1971**, *6*, 490.
(8) Kanig, G. *J. Cryst. Growth* **1980**, *48*, 303.
(9) Adams, W. W.; Yang, D.; Thomas, E. L. *J. Mater. Sci.* **1986**, *21*, 2239.
(10) Wignall, G. D.; Wu, W. *Polym. Commun.* **1983**, *54*, 354.
(11) Flory, P. J.; Yoon, D. Y. *Nature (London)* **1978**, *272*, 226.
(12) Sadler, D. M.; Barham, P. J. *Polymer* **1990**, *31*, 36.
(13) Chuah, H. H.; Lin, J. S.; Porter, R. S. *Macromolecules* **1986**, *19*, 2732.
(14) Hu, W. G.; Rohr, K. S. *Acta Polym.* **1999**, *50*, 271.
(15) Hiss, R.; Hobeika, S.; Lynn, C.; Strobl, G. *Macromolecules* **1999**, *32*, 4390.
(16) Koike, Y.; Cakmak, M. *Macromolecules* **2004**, *37*, 2171.
(17) Song, Y.; Nitta, K.; Nemoto, N. *Macromolecules* **2003**, *36*, 8066.
(18) Liu, T. M.; Juska, T. D.; Harrison, I. R. *Polymer* **1986**, *27*, 247.
(19) Unwin, A. P.; Bower, D. I.; Ward, I. M. *Polymer* **1985**, *26*, 1605.
(20) Ballard, D. G. H.; Cheshire, P.; Janke, E.; Nevin, A.; Schelten, J. *Polymer* **1982**, *23*, 1875.
(21) Sakurai, T.; Nozue, Y.; Kasahara, T.; Mizunuma, K.; Yamaguchi, N.; Tashiro, K.; Amemiya, Y. *Polymer* **2005**, *46*, 8846.
(22) Roberge, M.; Prud'homme, R. E.; Brisson, J. *Polymer* **2004**, *45*, 1401.
(23) Ogura, I.; Yamamoto, T. *Polymer* **1995**, *36*, 1375.
(24) Fougnies, C.; Damman, P.; Villers, D.; Dosiere, M.; Koch, M. H. J. *Macromolecules* **1997**, *30*, 1385.
(25) Rueda, D. R.; Garcia Gutierrez, M. C.; Ania, F.; Zolotukhin, M. G.; Balta, Calleja, F. J. *Macromolecules* **1998**, *31*, 8201.
(26) Samon, J. M.; Schultz, J. M.; Hsiao, B. S.; Seifert, S.; Stribeck, N.; Gurke, I.; Saw, C.; Collins, G. *Macromolecules* **1999**, *32*, 8121.
(27) Gazzano, M.; Focarete, M. L.; Riekel, C.; Scandola, M. *Biomacromolecules* **2000**, *1*, 604.
(28) Buleon, A.; Pontoire, B.; Riekel, C.; Chanzy, H.; Helbert, W.; Vuong, R. *Macromolecules* **1997**, *30*, 3952.
(29) Garcia Gutierrez, M. C.; Alfonso, G. C.; Riekel, C.; Azzurri, F. *Macromolecules* **2004**, *37*, 478.
(30) Nozue, Y.; Hirano, S.; Kurita, R.; Kawasaki, N.; Ueno, S.; Iida, A.; Nishi, T.; Amemiya, Y. *Polymer* **2004**, *45*, 8299.
(31) Riekel, C.; Karger-Kocsis, J. *Polymer* **1999**, *40*, 541.
(32) Kolb, R.; Wutz, C.; Stribeck, N.; von Krosigk, G.; Riekel, C. *Polymer* **2001**, *42*, 5257.
(33) Nozue, Y.; Kurita, R.; Hirano, S.; Kawasaki, N.; Ueno, S.; Iida, A.; Nishi, T.; Amemiya, Y. *Polymer* **2003**, *44*, 6397.
(34) Nozue, Y.; Hirano, S.; Kawasaki, N.; Ueno, S.; Yagi, N.; Nishi, T.; Amemiya, Y. *Polymer* **2004**, *45*, 8593.
(35) Amemiya, Y.; Ito, K.; Yagi, N.; Asano, Y.; Wakabayashi, K.; Ueki, T. *Rev. Sci. Instrum.* **1995**, *66*, 2290.
(36) Tate, M. W.; Chamberlain, D.; Gruner. S. M. *Rev. Sci. Instrum.* **2005**, *76*, 081301.
(37) Amemiya, Y.; Miyahara, J. *Nature (London)* **1988**, *336*, 89.
(38) Hughes, D. J.; Mahendrasingam, A.; Oatway, W. B.; Heeley, E. L.; Martin, C.; Fuller, W. *Polymer* **1997**, *38*, 6427.
(39) Shinohara, Y.; Kawasaki, N.; Ueno, S.; Kobayashi, I.; Nakajima, M.; Amemiya, Y. *Phys. Rev. Lett.* **2005**, *94*, 097801.
(40) Zambelli, A.; Locatelli, P.; Bajo, G.; Bovey, F. A. *Macromolecules* **1975**, *8*, 687.
(41) Inoue, K.; Oka, T.; Suzuki, T.; Yagi, N.; Takeshita, K.; Goto, S.; Ishikawa, T. *Nucl. Instrum. Methods* **2001**, *674*, A467−468.
(42) Keith, H. D.; Padden, Jr., F. J. *J. Appl. Phys.* **1966**, *37*, 4013.
(43) Keith, H. D.; Padden, Jr., F. J. *J. Appl. Phys.* **1973**, *44*, 1217.
(44) Hikosaka, M.; Seto, T. *Polym. J.* **1973**, *5*, 111.
(45) Shimamura, K.; Murakami, S.; Tsuji, M.; Katayama, K. *Nihon Rheol. Gakkai-shi* **1979**, *7*, 42.
(46) Hosoda, S.; Hori, H.; Yada, K.; Nakahara, S.; Tsuji, M. *Polymer* **2002**, *43*, 7451.

MA061924V